Astronomy & Astrophysics manuscript no. sdss February 2, 2008
(DOI: will be inserted by hand later)

arXiv:astro-ph/0307233v1 11 Jul 2003

Large Scale Structure in the SDSS DR1 Galaxy Survey

A. Doroshkevich[1,2], D.L. Tucker[3], S. Allam[3,4], and M.J. Way[1,5]

[1] Theoretical Astrophysics Center, Juliane Maries Vej 30, DK-2100 Copenhagen Ø, Denmark
[2] Keldysh Institute of Applied Mathematics, Russian Academy of Sciences, 125047 Moscow, Russia
[3] Fermi National Accelerator Laboratory, MS 127, P.O. Box 500, Batavia, IL 60510 USA
[4] National Research Institute for Astronomy & Geophysics, Helwan Observatory, Cairo, Egypt
[5] NASA Ames Research Center, Space Sciences Division, MS 245-6, Moffett Field, CA 94035, USA

Received ..., 2003/Accepted ..., 2003

Abstract. The Large Scale Structure in the galaxy distribution is investigated using The First Data Release of the Sloan Digital Sky Survey. Using the Minimal Spanning Tree technique we have extracted sets of filaments, of wall–like structures, of galaxy groups, and of rich clusters from this unique sample. The physical properties of these structures were then measured and compared with the statistical expectations based on the Zel'dovich' theory.
The measured characteristics of galaxy walls were found to be consistent with those for a spatially flat ΛCDM cosmological model with $\Omega_m \approx 0.3$ and $\Omega_\Lambda \approx 0.7$, and for Gaussian initial perturbations with a Harrison – Zel'dovich power spectrum. Furthermore, we found that the mass functions of groups and of unrelaxed structure elements generally fit well with the expectations from Zel'dovich' theory. We also note that both groups and rich clusters tend to prefer the environments of walls, which tend to be of higher density, rather than the environments of filaments, which tend to be of lower density.

Key words. cosmology: large-scale structure of the Universe: general — surveys

1. Introduction

With the advent of the Durham/UKST Galaxy Redshift Survey (DURS, Ratcliffe et al. 1996) and the Las Campanas Redshift Survey (LCRS, Shectman et al. 1996), the galaxy distribution on scales up to ∼300 h^{-1} Mpc could be studied. Now these investigations can be extended using the public data sets from The First Data Release of the Sloan Digital Sky Survey (SDSS DR1, Stoughton et al. 2002; Abazajian et al. 2003), which contains redshifts for ≈ 100 000 galaxies in four slices for distances $D \leq 600h^{-1}$Mpc.

The analysis of the spatial galaxy distribution in the DURS and the LCRS has revealed that the Large Scale Structure (LSS) is composed of walls and filaments, that galaxies are divided roughly equally into each of these two populations (with few or no truly isolated galaxies), and that richer walls are linked to the joint random network of the cosmic web by systems of filaments (Doroshkevich et al. 2000, 2001). Furthermore, these findings are consistent with results obtained for simulations of dark matter (DM) distributions (see e.g. Cole et al. 1998; Jenkins et al. 1998) and for mock galaxy catalogues based upon DM simulations (Cole et al. 1998).

The quantitative statistical description of the LSS is in itself an important problem. Beyond that, though, the analysis of rich catalogues can also provide estimates for certain cosmological parameters and for the characteristics of the initial power spectrum of perturbations. To do so, some theoretical models of structure formation can be used.

The close connection between the LSS and Zel'dovich' pancakes has been discussed by Thompson & Gregory (1978) and by Oort (1983). Now this connection is verified by the comparison of the statistical characteristics of observed and simulated walls with theoretical expectations (Demiański & Doroshkevich 1999, 2002, hereafter DD99 and DD02) based on the Zel'dovich theory of nonlinear gravitational instability (Zel'Dovich 1970; Shandarin & Zeldovich 1989). This approach connects the characteristics of the LSS with the main parameters of the underlying cosmological scenario and the initial power spectrum, and it permits the estimation of some of these parameters using the measured properties of walls. It was examined with the simulated DM distribution (DD99; Demiański et al. 2000), and was found that, for sufficiently representative samples of walls, a precision of better than 20% can be reached.

Effective methods of the statistical description of the LSS based on the Minimal Spanning Tree (MST) technique were developed by Demiański et al. (2000) and

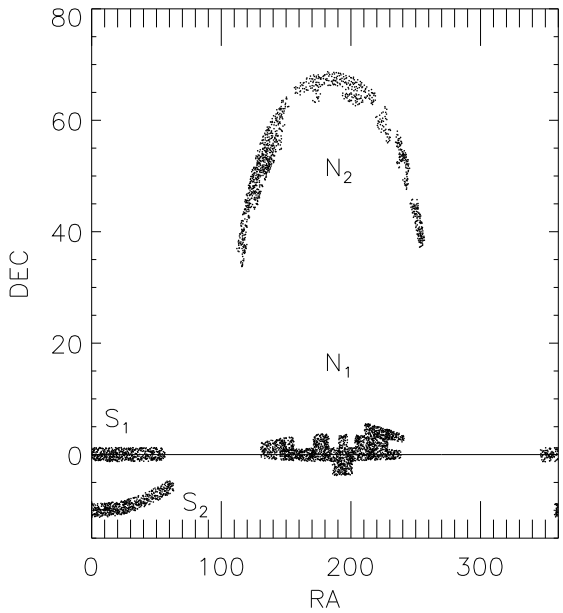

Fig. 1. Four regions of the DR1 sample on the sky.

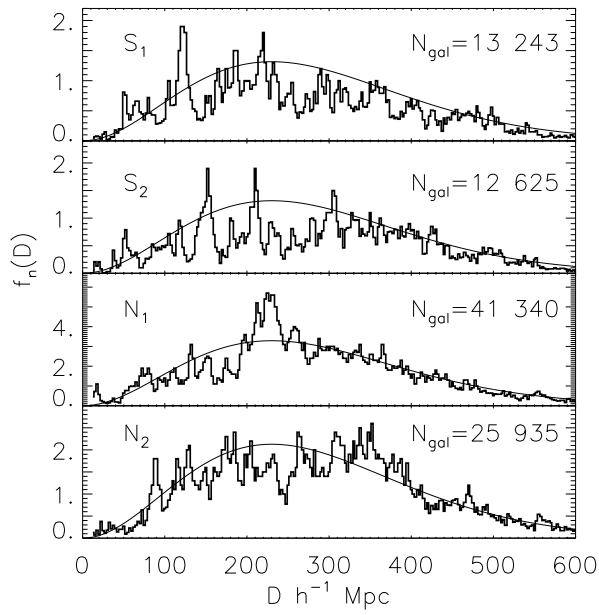

Fig. 2. The radial galaxies distributions in the four samples of the SDSS DR1. The selection function (1) is plotted by solid lines.

Doroshkevich et al. (2000, 2001), who applied them to DM simulations and to the DURS and the LCRS. These methods introduced in Barrow et al. (1985) and van de Weygaert (1991) generalize the popular "friends-of-friends" approach. In this paper we apply the same approach to the SDSS DR1, a sample from which we can obtain more representative and more precise measures of the properties of the LSS and the initial power spectrum of perturbations. Alternative methods based on Minkowski functionals are proposed by, for example, Schmalzing et al. (1999), or Sheth et al. (2002)

With the MST technique, we can quantitatively describe the sample under investigation and divide the sample into physically motivated subsamples of clusters with various threshold overdensities bounding them. Then we can extract the LSS elements and characterize their morphology. In particular, this technique allows us to discriminate between filamentary and wall–like structure elements located presumably within low and high density regions and to estimate their parameters for the different threshold overdensities. The same technique allows us to extract sets of high density groups of galaxies and to measure some of their properties.

The analysis of wall-like condensations is most informative. Comparison of the observed characteristics of walls with theoretical expectations (DD99; DD02) demonstrates that the observed galaxy distribution is consistent with Gaussianity initial perturbations and that the walls are the recently formed, partly relaxed Zel'dovich' pancakes. The mean basic characteristics of the walls are consistent with those theoretically expected for the initial power spectrum measured by the CMB observations summarized, for example, in Spergel et al. (2003).

In this paper we also analyse the mass functions of structure elements selected for a variety of boundary threshold overdensities. We show that these functions are quite similar to the expectations of Zel'dovich' theory, which generalizes the Press – Shechter formalism for any structure elements. In addition, the theory indicates that the interaction of large and small scale perturbations can be important for the formation of the observed LSS mass functions. Our analysis demonstrates that this interaction is actually seen in the influence of environment on the characteristics of groups of galaxies. This problem was also discussed in Einasto et al. (2003a,b).

This paper is organized as follows: In Secs. 2 we describe the sample of galaxies which we extracted from the SDSS DR1 and the method we have employed to correct for radial selection effects. In Sec. 3 we establish the general characteristics of the LSS. More detailed descriptions of the filamentary network and walls can be found in Secs. 4 and 5, respectively. In Secs. 6 and 7 we discuss the probable selected clusters of galaxies and the mass function of structure elements. We conclude with Sec. 8 where a summary and a short discussion of main results are presented.

2. The First Data Release of the Sloan Digital Sky Survey

We use as our observational sample the SDSS DR1 (Abazajian et al. 2003), which is the first public release of data from the SDSS (Fukugita et al. 1996; Gunn et al. 1998; York et al. 2000). The imaging data for the SDSS DR1 encompasses 2099 sq deg of sky. The DR1 also contains 186,240 follow up spectra, which are available over 1360 sq deg of the imaging data area. Galaxies are situated within two north fields, N_1 & N_2, and two south fields, S_1 & S_2. These regions are plotted in Fig. 1 .

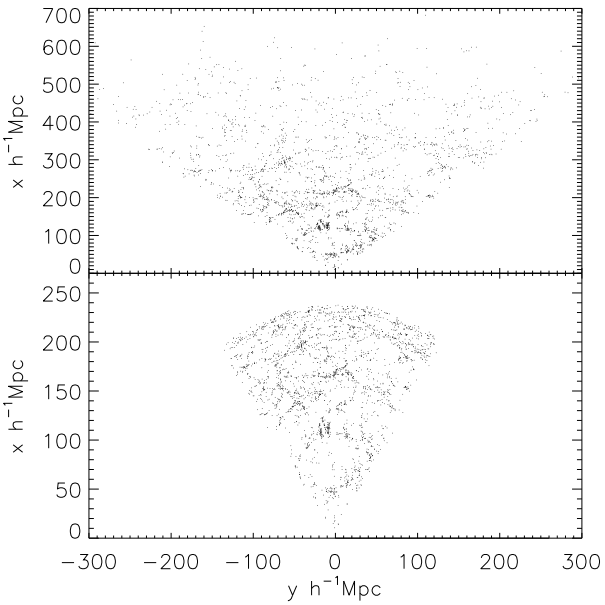

Fig. 3. The wedge diagram of galaxy distributions in the samples S_1 is real (top panel) and modified (bottom panel) radial coordinates.

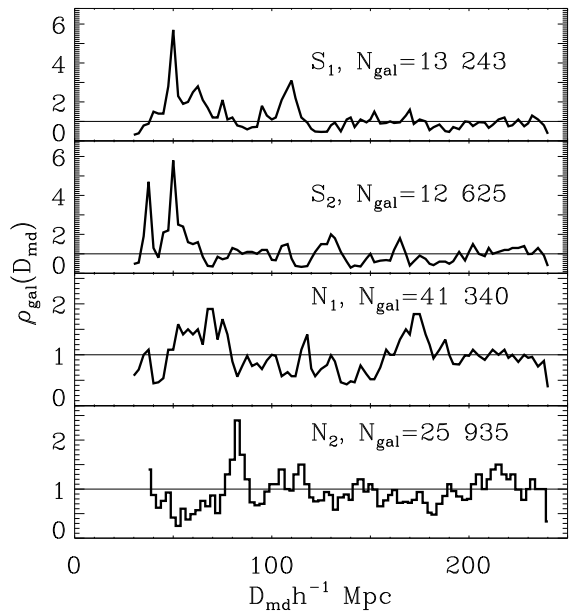

Fig. 4. The normalized mean galaxy density in the four modified samples of SDSS DR1.

We obtained our SDSS DR1 sample via the SDSS DR1 Spectro query server [1]. This is a web interface to the SDSS Catalog Archive Server. We selected all objects identified as galaxies with a 'redshift confidence minimal level' of 95% and no maximal level. No other constraints in the selection were made at this level.

Our method for detecting LSS depends on having largely contiguous regions. Hence we have removed some regions and artifacts from the DR1 sample. The following are the RA and DEC areas we masked out from the original DR1 query before our analysis:

- 174^h<RA<179^h, -4.0°<DEC<-1.22°
- 159^h<RA<163^h, 1.1°<DEC<4.0°
- 10^h<RA<50^h, 10°<DEC<20°
- 300^h<RA<355^h, -12°<DEC<-4°
- 250^h<RA<270^h, 52°<DEC<67°

2.1. Correction for radial selection effects

In Figure 2 we plot the radial distributions of galaxies in all four samples. In Figure 3 we plot the wedge diagramm of observed galaxy distribution for the sample S_1. As is clearly seen from these Figures, at distances $D \geq 400h^{-1}$Mpc this fraction of observed galaxies is strongly suppressed because of the radial selection effect. Note that this suppression is quite successfully fit by curves describing a selection function of the form

$$f_{gal}(D) \propto D^2 \exp[-(D/R_{sel})^{3/2}], \quad R_{sel} \approx 190h^{-1}\mathrm{Mpc} \quad (1)$$

[1] http://www.sdss.org/dr1

where D is a galaxy's radial distance and R_{sel} is the selection scale (Baugh & Efstathiou 1993). These fits are also plotted in Fig. 2.

In some applications, like when we want to correct a measure of the observed density to a measure of the true density, we would like to use equation (1) to correct for the radial selection effects after the fact. An example of such a case is calculating a group's or cluster's true richness based upon the observed number of galaxies it contains (Sec. 6 & 7). modified

In other applications, however, like in searching for groups or clusters in a magnitude-limited sample, we want to make a preemptive correction for the radial selection effects. For example, in a standard friends-of-friends percolation algorithm (e.g. Huchra & Geller 1982), this is done by adjusting the linking length as a function of radial distance. Here, instead, we employ the rather novel approach of adjusting the radial distances themselves as introduced and discussed in Doroshkevich et al. (2001). Hence, instead of the measured radial distance, we use a modified radial distance, D_{md}, where

$$D_{md}^3 = 2R_{sel}^3(1 - [1 + (D/R_{sel})^{3/2}] \exp[-(D/R_{sel})^{3/2}]) \quad (2)$$

The radial variations of the normalized number density of galaxies for all samples from Figure 2 are plotted in Figure 4. As is seen from this figure, the modified radial distances for the galaxies suppresses the very large-scale trends. On the other hand the relative position of galaxies remain unchanged and the smaller scale random variations in the density are emphasized. The wedge diagramm of modified galaxy distribution for the sample S_1 is also plotted in Fig. 3.

This correction does not change distances at $D \leq R_{sel}$ and is more important for the more distant regions of our samples ($D \geq 350h^{-1}$Mpc), which contain only ∼20% of

all galaxies. Thus, in the following analyses, we apply this correction only to the separation of the high and low density regions in the deeper samples. Of course, it cannot restore the lost information about the galaxy distribution in these regions, but it does help compensate for the strong drop in the observed galaxy density at these distances. It also allows one to apply the standard methods of investigation for the full catalogues with a depth of $600h^{-1}$Mpc.

3. General characteristics of observed large scale structure

To characterize the general properties of the large scale spatial galaxy distribution we use the Minimal Spanning Tree (MST) technique applied to both directly observed samples of galaxies and to samples corrected for the selection effect.

In our analysis here, we consider the four fields, plotted in Fig. 1, at the distance $D \leq 420h^{-1}$Mpc with

$$N_{gal} = 79\,183, \quad \langle n_{gal} \rangle \approx 10^{-2}\mathrm{Mpc}^{-3}\,, \tag{3}$$

where N_{gal} and $\langle n_{gal} \rangle$ are the total number of galaxies and the mean density of the samples. This sample contains ≈85% of all galaxies with moderate impact from selection effects. The numbers of galaxies in the separate fields are

- N_1, the northern sample (35 520 galaxies)
- N_2, the northern sample (21 983 galaxies)
- S_1, the southern sample (11 225 galaxies)
- S_2, the southern sample (10 455 galaxies)

3.1. The MST technique

The MST technique was first discussed by Barrow et al. (1985) and by van de Weygaert (1991). The MST is a construct from graph theory, originally introduced by Kruskal (1956) and Prim (1957), which has been widely applied in telecommunications and similar fields. It is a *unique network* associated with a given point sample and connects all points of the sample to a *tree* in a special and unique manner which minimizes the full length of the tree. Further definitions, examples, and applications of this approach are discussed in Barrow et al. (1985) and van de Weygaert (1991). More references to the mathematical results can also be found in van de Weygaert (1991).

One of earliest uses of MST approach in the study of large-scale structure was that of Bhavsar & Ling (1988), who successfully applied it to extract filamentary structures from the original CfA Redshift Survey. Its applications for the quantitative description of observed and simulated catalogues of galaxies were discussed in Demiański et al. (2000); Doroshkevich et al. (2000, 2001).

One of the most important features of the MST technique is generalization of the widely used "friends–of–friends" approach. It allows one to separate all clusters, LSS elements, with a given linking length. In spite of the very complex shape of the clusters, the linking length defines for each two points the local overdensity bounding the clusters with a relation familiar from "friends–of–friends" algorithms (Huchra & Geller 1982):

$$\delta_{thr} = 3/[4\pi\langle n_{gal}\rangle r_{lnk}^3]\,. \tag{4}$$

Further on it allows one to obtain characteristics of each cluster and of the sample of clusters forming the LSS with a given overdensity. Further discrimination can be performed for a given threshold richness of individual elements.

Here we will restrict our investigation to our results for the *probability distribution function of the MST edge lengths* $W_{MST}(l)$ and to the morphological description of individual clusters. The potential of the MST approach is not, however, exhausted by these applications.

3.2. Wall-like and filamentary structure elements

With the MST technique we can demonstrate that the majority of galaxies are concentrated within wall–like structures and filaments which connect walls to the joint random network of the cosmic web. The internal structure of both walls and filaments is complex. Thus, wall–like structures incorporate some fraction of filaments and both walls and filaments incorporate high density galaxy groups and clouds. In particular, clusters of galaxies are usually situated within richer walls while groups of galaxies are embedded within filaments. In spite of this, the galaxy distribution can be described as a set of one, two and three dimensional Poisson–like distributions. Naturally, a one dimensional distribution is more typical for filaments while two and three dimensional ones are typical for walls and groups of galaxies, respectively. As was shown in van de Weygaert (1991) Buryak & Doroshkevich (1996), a Poissonian distribution of galaxies within the LSS elements successfully reproduces the observed 3D correlation function of galaxies.

These result show that the probability distribution function of MST edge lengths (PDF MST), $W_{MST}(l)$, characterizes the geometry of the galaxy distribution. For 1D and 2D Poissonian distributions, typical for filaments and walls, $W_{MST}(l)$ is described by the following exponential and Rayleigh functions,

$$W_{MST}(l) = W_e(l) = \langle l\rangle^{-1}\exp(-l/\langle l\rangle)\,, \tag{5}$$

$$W_{MST}(l) = W_R(l) = 2l/\langle l^2\rangle\exp(-l^2/\langle l^2\rangle)\,.$$

These PDFs remain valid for any 1D and 2D distributions when the galaxy separation is small as compared with the curvature of the lines and surfaces. Comparison of measured and expected PDFs MST allows one to demonstrate the existence of these two types of structure elements and to make approximate estimates of their richness. Let us recall, however, that for the galaxy groups embedded within filaments, 2D and 3D Poissonian distributions are observed and, so, in this case we cannot see a purely 1D distribution. For walls this effect is less important because

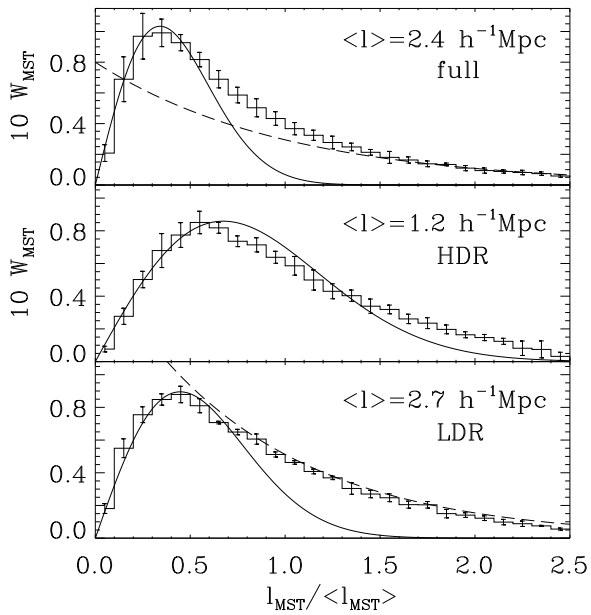

Fig. 5. PDFs of MST edge lengths in redshift space averaged over four samples are plotted for the full sample (top panel), HDRs (middle panel) and LDRs (bottom panel). Rayleigh and exponential fits are plotted by thin solid and dashed lines.

it only distorts the 2D distribution typical for such LSS elements.

In Fig. 5 (top panel) we plott the $W_{MST}(l_{MST})$'s for the entire sample of 79,183 galaxies situated at distances $D \leq 420h^{-1}$Mpc where, as is seen from Fig. 2, the impact of the selection effect is still moderate. The error bars show the scatter of measurements for the four subsamples. For each sample, N_1, N_2, S_1, S_2, we have

$$\langle l_{MST} \rangle = 2.5,\ 2.6,\ 2.3,\ 2.0\, h^{-1}\mathrm{Mpc}\,. \tag{6}$$

These variations demonstrate the differences in the sample properties (cosmic variance).

Notice in Fig. 5 that the $W_{MST}(l_{MST})$ is well fit by a superposition of Rayleigh (at $l_{MST} \leq \langle l_{MST} \rangle$) and exponential (at $l_{MST} \geq \langle l_{MST} \rangle$) functions. This confirms results discussed in Doroshkevich et al. (2000; 2001) in respect to the high degree of galaxy concentration within the population of high density rich wall–like structures and less rich filaments. However, as was noted in the same papers, with this approach the approximate separation of wall–like and filamentary structure elements can be performed only statistically. This is because the high density part of the PDF described by the Rayleigh function includes high density clouds situated in both filaments and walls. The exponential part of the PDF is related mainly to the filamentary component.

3.3. High and low density regions

The methods for an approximate statistical decomposition of a sample into subsamples of wall–like structures and filaments were proposed and tested in our previous publications (Demiański et al. 2000; Doroshkevich et al. 2000, 2001). The first step is to make a rough discrimination between the high and low density regions (HDRs and LDRs).

Such discrimination can be easily performed for a given overdensity contour bounding the clusters and a given threshold richness of individual elements. Following Doroshkevich et al. (2001), in all four samples with $D \leq 420h^{-1}$Mpc, wall–like high density regions (HDRs) were identified with clusters found for a threshold richness $N_{thr} = 40$ and a threshold overdensity contour bounding the cluster equal to the mean density, $\delta_{thr} = 1$. These samples, N_1, N_2, S_1, S_2, of HDRs contain 49%, 47%, 51% and 47% of all galaxies. The samples of low density regions (LDRs), which are occupied mainly by filaments and poor groups of galaxies, are complementary to the HDRs in that the LDRs are simply the leftovers from the original total samples after the HDRs have been removed.

In Figure 5 (middle panel) the $W_{MST}(l)$ plotted for the HDRs is very similar to a Rayleigh function, thus confirming with this criterion the sheet-like nature of the observed galaxy distribution within the HDRs. As before, the error bars show the scatter of measurements for the four subsamples. For 90% of objects we have

$$W_{HDR} = (1 \pm 0.18)\ W_R, \quad l_{MST} \leq 1.65\langle l_{MST} \rangle\,, \tag{7}$$

where W_R is the Rayleigh function (5). Larger difference between observed and expected PDFs for larger l_{MST} indicates that the selected sample of HDRs includes some fraction of objects, $\sim 10\%$, which can be related to the filamentary component with the exponential PDF.

For the LDRs, the $W_{MST}(l)$ is plotted in Fig. 5 (bottom panel). For small edge lengths, $l \leq \langle l_{MST} \rangle$, it also fits well to a Rayleigh function indicating that $\sim 60\%$ of LDR galaxies are concentrated within less massive 3D (elliptical) and 2D (sheet-like) clouds. This result confirms the strong disruption of filaments to a system of high density clouds. For larger edge lengths, however, the LDR $W_{MST}(l)$ appears to be closer to an exponential function, indicating that according to this criterion the spatial distribution of the remaining $\sim 40\%$ of LDR galaxies is similar to a 1D Poissonian one which is typical for filamentary structures.

The mean edge lengths, $\langle l_{MST} \rangle$, found for HDRs and LDRs in samples N_1, N_2, S_1, S_2 are

$$\langle l_{MST} \rangle = 1.2,\ 1.3,\ 1.2,\ 1.3\, h^{-1}\mathrm{Mpc}\,, \tag{8}$$

$$\langle l_{MST} \rangle = 2.8,\ 2.7,\ 2.6,\ 2.8\, h^{-1}\mathrm{Mpc}\,. \tag{9}$$

These values differ by about a factor of two from each other, indicating that, as is seen from (4), the difference in the mean density within HDRs and LDRs elements is about an order of magnitude. Of course, the volume averaged density of LDRs is still less.

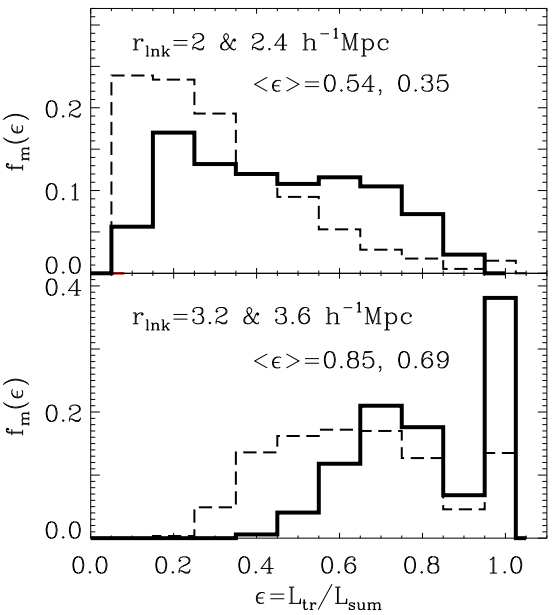

Fig. 6. Mass functions of structure elements, $f_m(\epsilon)$, $\epsilon = L_{tr}/L_{sum}$ for the structure elements selected within HDRs (top panel, solid and dashed lines) and within LDRs (bottom panel, solid and dashed lines).

3.4. Morphology of the structure elements

Within so defined HDRs and LDRs themselves we can extract with the MST technique subsamples of structure elements for various threshold overdensities. We can then suitably characterize the morphology of each structure element by comparing the sum all edge lengths within its full tree, L_{sum}, with the sum of all edge lengths within the tree's trunk, L_{tr}, which is the longest path that can be traced along the tree without re-tracing any steps. The ratio of these lengths

$$\epsilon = L_{tr}/L_{sum}\,. \tag{10}$$

suitably characterizes the morphology of the LSS elements.

For filaments, we can expect that the lengths of the full tree and of the trunk are similar to each other, $\epsilon \sim 1$, whereas for clouds and walls these lengths are certainly very different and $\epsilon \leq 1$. This approach takes into account the internal structure of each element rather than the shape of the isodensity contour bounding it, and in this respect it is complementary to the Minkowski Functional technique (e.g. Schmalzing et al. 1999; Sheth et al. 2002).

However, even this method cannot discriminate between the wall–like and 3D (elliptical) clouds and those rich filaments having many long branches for which again $\epsilon \leq 1$. This means that both the PDF of this ratio, $W(\epsilon)$, and the corresponding mass function, $f_m(\epsilon)$, are continuous functions and the morphology of structure elements can be more suitably characterized by the degree of filamentarity and 'wall-ness'. This also means that we can only hope to distinguish statistical differences between the morphologies of structure elements in HDRs and the morphologies of structure elements in LDRs.

The selection of clusters within HDRs and LDRs was performed for two threshold linking lengths, $r_{lnk} =$ 2. & $2.4h^{-1}$Mpc for HDRs, and $r_{lnk} = 3.2$ & $3.6h^{-1}$Mpc for LDRs. These values are larger than the mean edge lengths and characterize the LSS elements with intermediate richness when the measured difference between the walls and filaments is maximal. As was noted above, for lower linking lengths this method characterizes mainly the internal structure of the LSS elements while for large linking lengths filaments percolate and form the joint network with again $\epsilon \ll 1$.

The distribution functions of the ratio, $W(\epsilon)$, are found to be close to Gaussian with $\langle\epsilon\rangle \approx 0.5$ & 0.70 for HDRs and LDRs, respectively. The mass functions, $f_m(\epsilon)$, plotted in Fig. 6 for the same linking lengths are shifted to the left (for HDRs) and to the right (for LDRs) with respect to the middle point. Differences between these functions found for smaller and larger linking lengths illustrate the impact of the percolation process and disruption of the LSS elements.

These results verify the objective nature of the differences in the structure morphologies in HDRs and LDRs.

4. Statistical characteristics of filaments

Theoretical characteristics of the LSS elements relate to the dominant dark matter (DM) component while the observed galaxy distribution relates to the luminous matter which represent only $\sim 3 - 5\%$ of the mean density of the Universe. Spatial distribution of dark and luminous matter is strongly biased. None the less, some observed characteristics of filamentary components of the LSS can be compared with both available theoretical expectations and characteristics obtained for simulated DM distributions.

The most interesting ones are the PDF of the linear density of filaments measured as the mass or number of objects per unit length of filament, Σ_{fil}. The other is the mean surface density of filaments σ_{fil}, defined as the mean number of filaments intersecting a unit area of arbitrary orientation. Both characteristics depend upon the threshold linking length, r_{lnk}, used for the filament selection and upon the threshold richness of filaments. However, both characteristics are independent from the small scale clustering of matter within filaments.

Comparison of these characteristics of filaments for observed and simulated catalogues allows one to test the cosmological model used. However, the connection of quantitative characteristics of filaments with the initial power spectrum is complex and these measurements cannot yet be used for estimates of the power spectrum.

4.1. Linear density of filaments

As was found in DD99 and DD02, for the CDM–like initial power spectrum the PDF of the filament linear density can

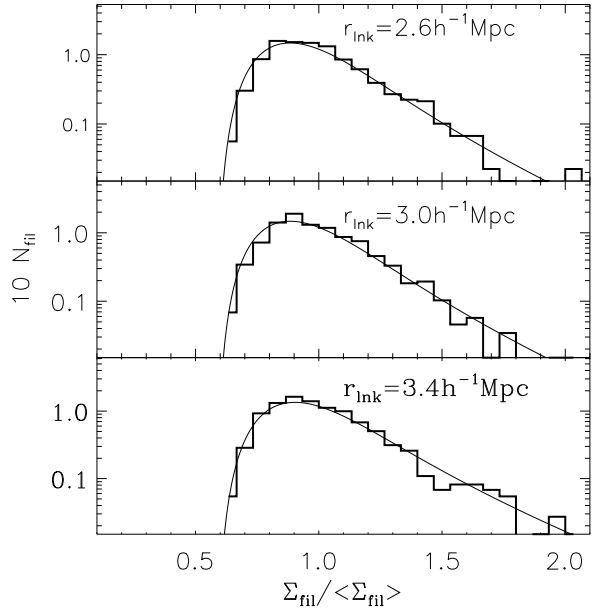

Fig. 7. Distribution function, N_{fil}, for the linear density of 'galaxies' along a tree for filaments selected in LDRs of the mock catalogues with three linking lengths. Fits (11) are plotted by solid lines.

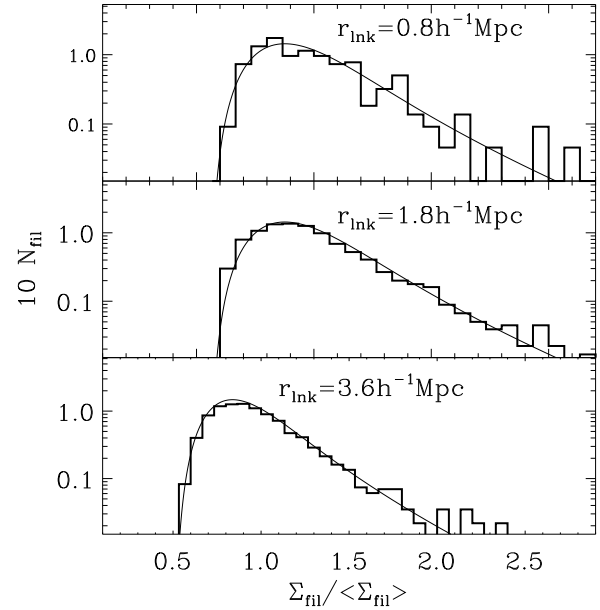

Fig. 8. Distribution function, N_{fil}, for the linear density of galaxies along a tree for filaments selected in LDRs of the DR1 with three linking lengths. Fits (11) are plotted by solid lines.

be written as follows:

$$N_{fil}\ d\Sigma_{fil} \approx \frac{1.5}{\langle\Sigma_{fil}\rangle} \exp(-\sqrt{3\Sigma_{fil}/\langle\Sigma_{fil}\rangle})\ d\Sigma_{fil}\,. \qquad (11)$$

However, poorer filaments cannot actually be selected in either simulated or observed catalogues. Hence, even for high resolution simulations the measured PDF is well fitted by the relation

$$N_{fil} \approx a_0\ \mathrm{erf}^4[a_1(x-x_0)] \exp[-\sqrt{a_2(x-x_0)}] \qquad (12)$$

where $x = \Sigma_{fil}/\langle\Sigma_{fil}\rangle, x_0 \approx 0.35, a_1 \approx 2-2.5$ and $a_2 \approx 30-40$ (DD02) and $\langle\Sigma_{fil}\rangle \sim 3/r_{lnk}$. Here the cutoff of the PDF at $x = x_0$ reflects the limited resolution of simulated matter distribution.

These results can be compared with ones obtained for for the DR1 and the mock catalogue (Cole et al. 1998) which allows one to estimate the impact of the selection effect for the measured linear density of filaments. In both the cases, the linear density of objects was measured by the ratio of the number of points and the length of the MST for each filaments of the sample.

For the mock catalogue the PDFs of the linear density of filaments are plotted in Fig. 7 for three linking length (with $\delta_{thr} \approx 1,\ 0.7$ & 0.5). These PDFs are well fitted by expression (12) for parameters $x_0 \approx 0.6, a_1 \approx 2.5, a_2 \approx 80-90$. For all linking lengths we get $\langle\Sigma_{fil}\rangle r_{lnk} = 2.25 \pm 0.04$. For the observed DR1 catalogue the same PDFs are plotted in Fig. 8 also for three linking length (with $\delta_{thr} \approx 50,\ 5$ & 0.55). They are well fitted by the same expression (12) for parameters $x_0 \approx 0.5, a_1 \approx 2.5, a_2 \approx 70-80$. For this sample we get $\langle\Sigma_{fil}\rangle r_{lnk} = 2.2 \pm 01$.

These results show that, in all the cases, the measured PDFs are well fit by the same expression (12) which coincides with the theoretically expected one (11) at $\Sigma_{fil} \geq \langle\Sigma_{fil}\rangle$. The mean linear density, $\langle\Sigma_{fil}\rangle$, clearly depends upon the linking length used for filament selection. The selection effect increases the product $\langle\Sigma_{fil}\rangle r_{lnk}$ by ~ 1.5 times as compared with results obtained for the DM simulations.

These results show that the observed galaxy distribution nicely represents the expected and simulated ones. The results also indicate that the general properties of filaments are consistent with a CDM–like initial power spectrum.

4.2. Typical size of the filamentary network

Due to the complex shape of the network of filaments spanning the LDRs any definition of the typical size of a network cell is mearly convenient. As was discussed in Doroshkevich et al. (2001), two definitions seem to be the most objective. One is the mean free path between filaments along a random straight line. The other is the mean distance between branch points of the tree along the trunk of selected filaments. The second definition tends to yield cell sizes that are typically a factor of 1.5 smaller than those yielded by the mean-free-path definition.

Theoretical estimates of this size are uncertain because it strongly depends upon the sample of selected filaments (DD02). This means that this characteristic strongly depends upon the catalogue used. Moreover, filaments are connected to the network only for larger linking lengths; thus the typical measured cell size depends also upon the threshold linking length used. Hence, for the LCRS the mean free path between filaments with a

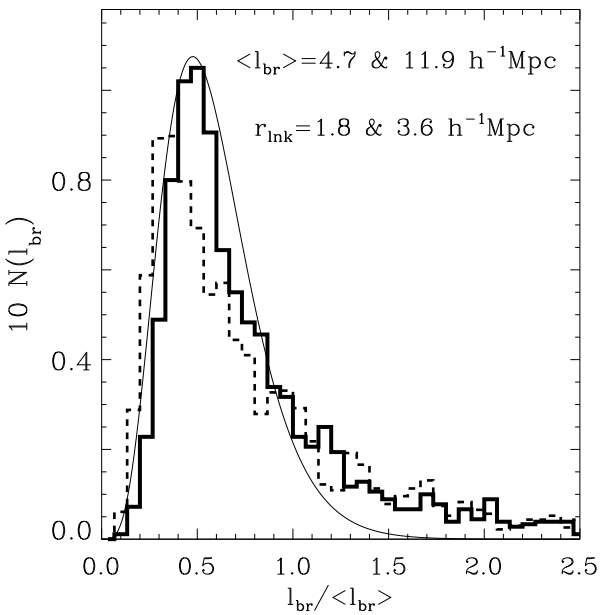

Fig. 9. Distribution functions, N, for the distance between branch points along a trunk for filaments selected in LDRs (thick solid and dashed lines). Fit (13) is plotted by thin solid line.

variety of richness was estimated in Doroshkevich et al. (2001) as $\sim 13-30h^{-1}$Mpc. The mean distance between branch points of the tree along the trunk was estimated as $\approx 10h^{-1}$Mpc and it rapidly increases with the linking length used owing the progressive percolation of filaments and formation of the joint LSS network.

Here with a richer sample of filaments we can also estimate the PDFs of the cell sizes measured by the distance between branch points of the tree along the trunk. These PDFs, $N(l_{br})$, are plotted in Fig. 9 for two linking lengths, $r_{lnk} = 1.8$ & $3.6h^{-1}$Mpc, which correspond to the threshold overdensities $\delta_{thr} = 0.66$ & 0.5. These PDFs are roughly fitted by expression

$$N(l_{br}) \approx 270x^{4.5}\exp(-9.1x), \quad x = l_{br}/\langle l_{br}\rangle\,, \tag{13}$$

The measured mean distance between branch points,

$$\langle l_{br}\rangle \approx 4.7 \;\&\; 11.9h^{-1}\mathrm{Mpc}\,.$$

are close to those obtained in Doroshkevich et al. (2001) and Doroshkevich et al. (1996) and those cited above. For smaller r_{lnk} this estimate is decreased because of the domination of short filaments which are not yet connected to the network.

5. Parameters of the wall–like structure elements

The statistical characteristics of observed walls were first measured using the LCRS and DURS (Doroshkevich et al. 2000, 2001). The rich sample of walls extracted from the SDSS DR1, however, permits more refined estimates of these characteristics. As was discussed in Sec. 3.2 walls dominate the HDRs, and thus these subsamples of galaxies can be used to estimate the wall properties.

The expected characteristics of walls and methods of their measurement were discussed in Demiański et al. (2000) so here we will only briefly reproduce the main definitions. It is important that these characteristics can be measured independently in radial and transverse directions, which reveals the strong influence of the velocity dispersion on other wall characteristics.

5.1. Main wall characteristics

Main characteristic of walls is their mean dimensionless surface density, $\langle q_w\rangle$, measured by the number of galaxies per Mpc^2 and normalized by the mean density of galaxies multiplied by a coherent length of the initial velocity field (DD99; DD02)

$$l_v \approx 33h^{-1}\mathrm{Mpc}\;(0.2/\Gamma), \quad \Gamma = \Omega_m h\,, \tag{14}$$

where Ω_m is the mean matter density of the Universe. For Gaussian initial perturbations, the expected probability distribution function (PDF) of the surface density is

$$N_{th}(q_w) = \frac{1}{\sqrt{2\pi}}\frac{1}{\tau_m\sqrt{q_w}}\exp\left(-\frac{q_w}{8\tau_m^2}\right)\mathrm{erf}\left(\sqrt{\frac{q_w}{8\tau_m^2}}\right)\,, \tag{15}$$

$$\langle q_{th}\rangle = 8(0.5+1/\pi)\tau_m^2 \approx 6.55\tau_m^2\,.$$

This relation links the mean surface density of walls with the dimensionless amplitude of perturbations, τ_m,

$$\tau_m = \sqrt{\langle q_w\rangle/6.55}\,, \tag{16}$$

which can be compared with those measured by other methods (DD02, Sec. 8.2).

Other important characteristics of walls are the mean velocity dispersion of galaxies within walls, $\langle w_w\rangle$, the mean separation between walls, $\langle D_{sep}\rangle$, the mean overdensity, $\langle\delta\rangle$, and the mean thickness of walls, $\langle h\rangle$. The mean velocity dispersion of galaxies, $\langle w_w\rangle$, can be measured in radial direction only whereas other wall characteristics can be measured both radially and along transverse arcs. Comparison of the wall thickness and the overdensity, $\langle h\rangle$ and $\langle\delta\rangle$, measured in transverse (t) and radial (r) directions, illustrates the influence of the velocity dispersion of galaxies on the observed wall thickness.

The velocity dispersion of galaxies within a wall w_w can be related to the radial thickness of the wall by this relation (Demiański et al. 2000):

$$h_r = \sqrt{12}H_0^{-1}w_w\,. \tag{17}$$

For a relaxed, gravitationally confined wall, the measured wall overdensity, surface density, and the velocity dispersion are linked by the condition of static equilibrium. Consider a wall as a slab in static equilibrium, and this slab has a nonhomogeneous matter distribution across it. We can then write the condition of static equilibrium as follows:

$$w_w^2 = \frac{\pi G\mu^2}{\langle\rho\rangle\delta}\Theta_\Phi = \frac{3}{8}\frac{\Omega_m}{\delta}(H_0 l_v q_w)^2\Theta_\Phi\,, \tag{18}$$

Here $\mu = \langle\rho\rangle l_v q_w$ is the mass surface density of the wall and the factor $\Theta_\Phi \sim 1$ describes the nonhomogeneity of the matter distribution across the slab. Unfortunately, for these estimates we can only use the velocity dispersion and overdensity measured for radial and transverse directions. Hence, the final result cannot be averaged over the samples of walls.

5.2. Measurement of the wall characteristics

The characteristics of the walls can be measured with the two parameter core–sampling approach (Doroshkevich et al. 1996) applied to the subsample of galaxies selected within HDRs. With this method, all galaxies of the sample are distributed within a set of radial cores with a given angular size, θ_c, or within a set of cylindrical cores oriented along arcs of right ascension with a size d_c. All galaxies are projected on the core axis and collected to a set of one-dimensional clusters with a linking length, l_{link}. The one-dimensional clusters with richnesses greater than some threshold richness, N_{min}, are then used as the required sample of walls within a sampling core.

Both the random intersection of core and walls and the nonhomogeneous galaxy distribution within walls lead to significant random scatter of measured wall characteristics. The influence of these factors cannot be eliminated, but it can be minimized for an optimal range of parameters θ_c, d_c, l_{link} and N_{min}. Results discussed below are averaged over the optimal range of these parameters.

For the measurement of wall characteristics in the radial direction four samples of HDRs galaxies were used in each field of the DR1 catalogue. One of these samples was selected as was discussed in Sec. 3.3, three other samples were selected from the catalogues *already corrected for radial selection effects* (Sec. 2.1) with the same threshold overdensity $\delta_{thr} = 1$ and for HDRs containing $\sim$ 43%, 50%, and 56% of all galaxies in the field. In all the cases, the wall parameters were measured in real space for the selected samples of the HDRs. The mean wall properties were averaged over four radial core sizes ($\theta_c = 2^\circ, 2.25^\circ, 2.5^\circ$ and 2.75°) and for six core-sampling linking lengths ($2h^{-1}$Mpc$\leq l_{link} \leq 4.5h^{-1}$Mpc). Final averaging was performed over all sixteen samples and over all θ_c and l_{link}.

Due to the complex shape of the fields S_2 and N_2, the measurements of wall characteristics in the transverse direction were performed for the fields S_1 and N_1 only. The mean wall properties were averaged over four core diameters ($d_c = 6.0$, 6.5, 7.0, and 7.5 h^{-1}Mpc) and five core-sampling linking lengths ($2h^{-1}$Mpc $\leq l_{link} \leq 4.h^{-1}$Mpc).

5.3. Measured characteristics of walls

The mean radial and tranverse wall properties for all fields are listed separately in Table 1. Characteristics obtained by averaging over all samples are compared with those from the DURS and LCRS and with those from mock catalogues simulating the SDSS EDR (Cole et al. 1998). Both DM simulation and mock catalogues are prepared for the ΛCDM cosmological model with $\Omega_m = 0.3$, $\Omega_\Lambda = 0.7$ and with the amplitude of perturbations $\sigma_8 = 1.05$ that exceed the now accepted value $\sigma_8 = 0.9\pm0.1$ (Spergel et al. 2003). This excess of the amplitude increases both the measured τ_m and $\langle q\rangle$ by $\sim$ 10% and $\sim$ 20%, respectively.

The richness and geometry of these catalogues are strongly different. Thus, DURS is an actual 3D catalogue but it contains $\sim$ 2 500 galaxies at the distance $D \leq 250h^{-1}$ Mpc and its representativity is strongly limited. The LCRS include $\sim$ 21 000 galaxies at the distance $D \leq 450h^{-1}$ Mpc but they are distributed within six thin slices that again distorts the measured wall characteristics. Moreover, both catalogues include a small number of walls with large scatter in richness. This leads to a significant scatter of measured characteristics of walls for these catalogues which is a manifestation of well known cosmic variance. Only with an actually representative catalogue such as the the SDSS can this effect can be suppressed.

The difference between the mean wall surface densities measured for $\sim$ 15–20% of samples reflects real variations in wall properties for a limited portion of the samples. However, the scatters of mean values listed in Table 1 partially include the dispersions depending on the shape of their distribution functions. The actual scatter of the mean characteristics of walls averaged over all samples listed in Table 1 is also $\leq$ 10–12%.

The amplitude of initial perturbations characterized by values τ_m for the richer sample measured in the radial direction is

$$\tau \approx (0.53 \pm 0.05)\sqrt{\Gamma} = (0.24 \pm 0.02)\sqrt{\frac{\Gamma}{0.2}}\,. \qquad (19)$$

This is quite consistent with estimates found for simulations. Differences between this value and τ_m measured in the transverse direction for the DR1, the LCRS and the DURS demonstrate the impact of the representativity of the catalogue used.

The difference between the wall thickness measured in the radial and transverse directions, h_r and h_t, indicates that, along a short axis, the walls are gravitationally confined stationary objects. Just as with the 'Finger of God' effect for clusters of galaxies, this difference characterizes the gravitational potential of compressed DM rather than the actual wall thickness. The same effect is seen as a difference between the wall overdensities measured in radial and transverse directions.

The difference between the wall thicknesses is compared with the velocity dispersions of galaxies within the walls, $\langle w_w\rangle$. Clusters of galaxies with large velocity dispersions incorporated in walls also increase the measured velocity dispersion. The correlation between the wall surface density and the velocity dispersion confirms the relaxation of matter within walls. This relaxation is probably accelerated due to strong small scale clustering of matter within walls.

Table 1. Wall properties in observed and simulated catalogues

sample	N_{gal}	$\langle q_w\rangle/\Gamma$	$\tau_m/\sqrt{\Gamma}$	$\langle\delta_r\rangle$	$\langle\delta_t\rangle$ h^{-1}Mpc	$\langle h_r\rangle$ h^{-1}Mpc	$\langle h_t\rangle$ km/s	$\langle w_w\rangle$ h^{-1}Mpc	$\langle D_{sep}\rangle$
radial cores									
N1	41 217	2.01 ± 0.21	0.55 ± 0.03	1.3	-	10.2 ± 1.9	-	295 ± 55	69 ± 14
N2	25 935	1.61 ± 0.16	0.49 ± 0.03	1.1	-	10.5 ± 2.0	-	303 ± 57	78 ± 17
S1	13 215	2.21 ± 0.19	0.58 ± 0.03	1.4	-	10.5 ± 1.7	-	303 ± 50	67 ± 14
S2	12 585	1.79 ± 0.33	0.51 ± 0.04	1.3	-	9.0 ± 1.8	-	260 ± 50	83 ± 20
transverse cores for the SDSS DR1									
N1	16 883	2.47 ± 0.51	0.61 ± 0.07	-	3.9	-	4.3 ± 0.8	-	65 ± 11
S1	13 215	2.29 ± 0.64	0.58 ± 0.08	-	3.9	-	4.0 ± 0.8	-	58 ± 11
observed samples									
SDSS (radial)	92 952	1.91 ± 0.32	0.53 ± 0.05	1.3	-	10.1 ± 2.0	-	291 ± 56	74 ± 17
SDSS (transverse)	29 311	2.42 ± 0.67	0.60 ± 0.08	-	3.5	-	4.9 ± 1.3	-	64 ± 14
LCRS	16 756	2.51 ± 0.9	0.62 ± 0.10	3.0	7.4	8.6 ± 0.8	2.8 ± 0.7	247 ± 48	60 ± 10
DURS	2 500	2.23 ± 0.6	0.58 ± 0.08	1.7	6.5	9.7 ± 1.8	4.9 ± 1.2	280 ± 52	44 ± 10
mock catalogues in real and redshift spaces for the model with $\Gamma = 0.2$									
redshift	98 828	2.7 ± 0.5	0.63 ± 0.06	1.8	3.8	11.8 ± 2.1	6.5 ± 1.4	338 ± 65	50 ± 10
real	98 828	2.1 ± 0.4	0.57 ± 0.06	4.3	4.6	4.8 ± 1.0	4.2 ± 1.0	305 ± 47	50 ± 10
DM catalogue in real space for the model with $\Gamma = 0.2$									
real	$7.1 \cdot 10^6$	2.5 ± 0.4	0.63 ± 0.04	2.7		4.9 ± 0.5		245 ± 30	52 ± 5

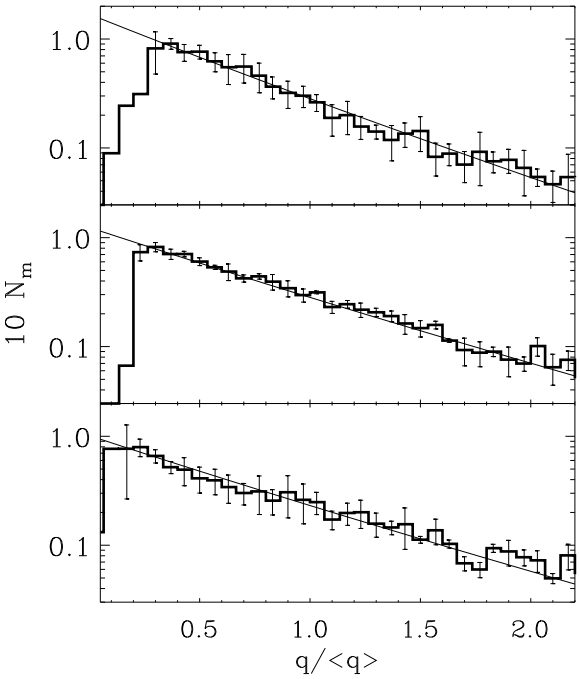

Fig. 10. The PDFs of dimensionless surface density of walls, $N_m(q/\langle q\rangle)$, for walls selected in the DM simulation (top panel) and the mock catalogue in real (middle panel) and redshift (bottom panel) spaces. Fits (15) are plotted by solid lines.

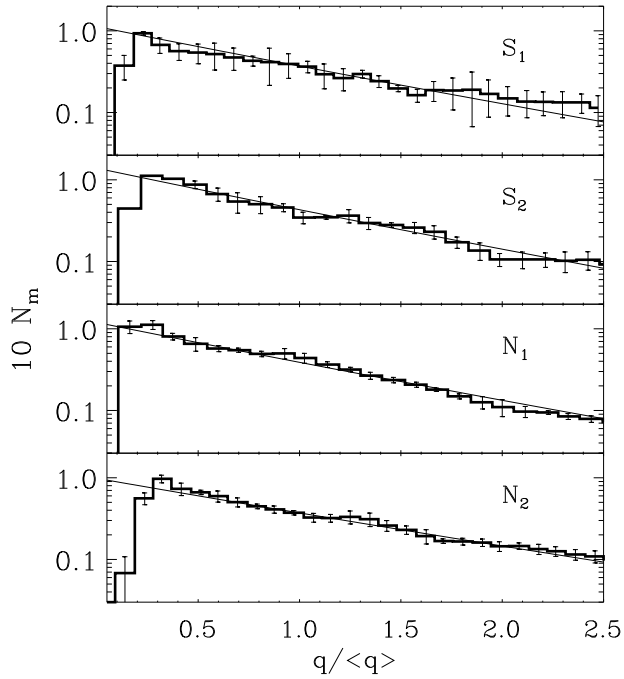

Fig. 11. The PDFs of observed dimensionless surface density of walls, $N_m(q/\langle q\rangle)$, for walls selected in four regions of the SDSS galaxy catalogues. Theoretically expected fits are plotted by solid lines.

The measured PDFs of the surface density of walls are plotted in Figs. 10 and 11 for the simulated DM distribution, mock catalogues in real and redshift spaces, and four observed samples of the SDSS DR1. These are nicely fit by the expected expression (15). Thus, for simulated samples we have, respectively,

$$N_m = (1 \pm 0.1)N_{th}, \quad \langle q\rangle/\langle q_{th}\rangle = 0.78, 0.87, 0.87\,, \qquad (20)$$

where N_{th} and $\langle q_{th}\rangle$ are given by (15). For the two southern samples of the SDSS DR1 we get:

$$N_m = (1.1 \pm 0.2)N_{th}, \quad \langle q\rangle/\langle q_{th}\rangle = 1.07\,, \qquad (21)$$

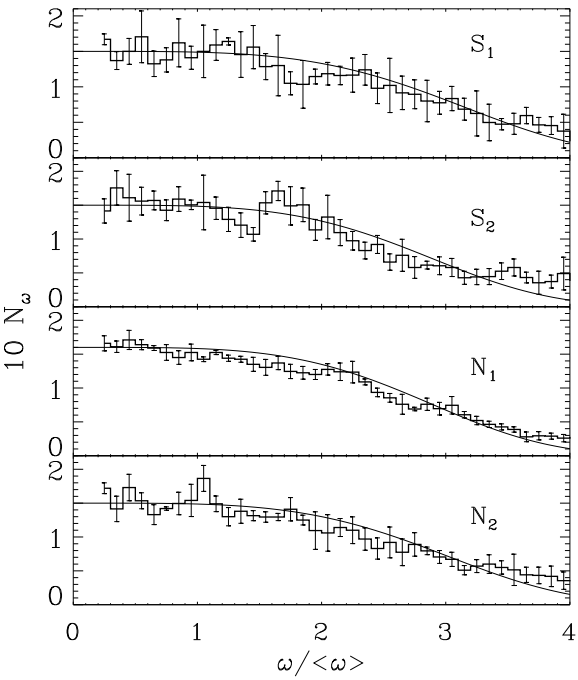

Fig. 12. The PDFs, $N_w(w/\langle w\rangle)$, of reduced velocity dispersion within wall (24) for walls selected in four regions of the SDSS galaxy catalogues. Gaussian fits are plotted by solid lines.

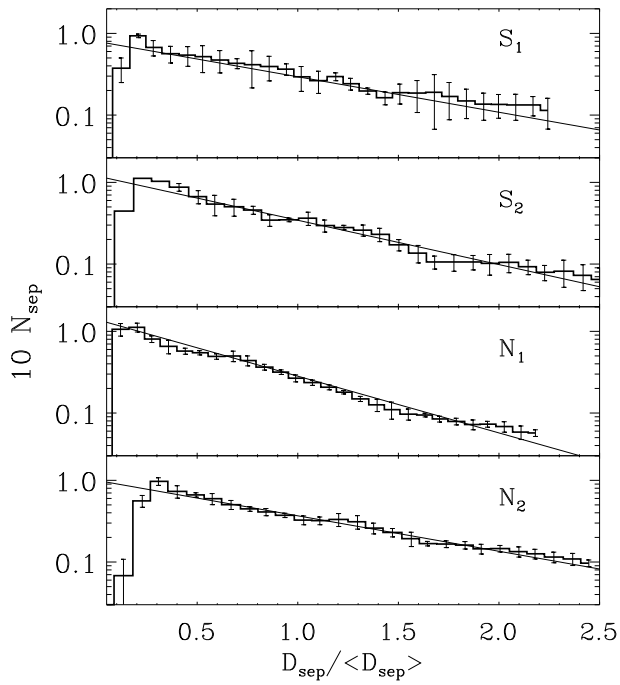

Fig. 13. The PDFs, $N_{sep}(D_{sep}/\langle D_{sep}\rangle)$, of observed wall separations for walls selected in four regions of the SDSS galaxy catalogues. Theoretically expected for the Possonian distribution exponential fits are plotted by solid lines.

and for the two northern samples of the SDSS DR1 we get:

$$N_m = (1. \pm 0.1)N_{th}, \quad \langle q\rangle/\langle q_{th}\rangle = 0.97\,, \tag{22}$$

These results verify that, the observed walls represent recently formed Zel'dovich' pancakes.

Using the measured mean wall overdensity in the transverse direction listed in Table 1 we have for the parameter Θ_Φ introduced in equation (18)

$$\Theta_\Phi \approx \frac{\langle\delta\rangle}{3}\frac{0.3}{\Omega_m} \approx 1.1\,, \tag{23}$$

which is also consistent with the expected values for relaxed and stationary walls.

As was proposed in Demiański et al. (2000) we can discriminate between systematic variations in the measured velocity dispersion due to regular variations in the surface density along the walls (Fig. 11) and the random variations in the velocity dispersion which integrates the evolutionary history of each wall. Indeed, along a shorter axis, for gravitationally bound and relaxed walls we can expect that

$$w_w^2 \propto q^2/\delta \propto \delta^{\gamma-1}, \quad w_w \propto q^{1-1/\gamma}\,.$$

Here we assume that the distribution of DM component and galaxies can be approximately described by the polytropic equation of state with the power index $\gamma \approx 5/3$ – 2. Demiański et al. (2003) suggest for consideration a reduced velocity dispersion, ω_w,

$$\omega_w = |\ln(w_w q_w^{-p_w})|, \quad p_w \approx 1 - 1/\gamma \approx 0.5\,, \tag{24}$$

corrected for variations of the wall thickness. For this function the systematic variations of w_w are essentially suppressed and, in most respects, it is similar to the entropy of compressed matter. It integrates the action of random factors in the course of wall formation. Hence, for this function the Gaussian PDF, N_ω, can be expected. Indeed, this PDF plotted in Fig. 12 for four samples of the SDSS DR1 is quite similar to a Gaussian function with a standard deviation $\sigma_\omega \approx 2.25\langle\omega\rangle$. These results show a large scatter of evolutionary histories of observed walls.

Note that, for all the samples listed in Table 1, the mean wall separation, $\langle D_{sep}\rangle$, is close to twice that of the coherent length of the initial velocity field,

$$\langle D_{sep}\rangle \approx 2l_v\,, \tag{25}$$

for the low density cosmological models with $\Gamma \approx 0.2$ (14). These results coincide with the estimates of the matter fraction, $\sim 50\%$, accumulated within walls. Due to the large separation of walls, the correlations of their positions is small and a random 1D Poissonian PDF of the separation can be expected. These PDFs are plotted in Fig. 13 together with the exponential fits.

Finally, we would like to draw attention to the fact that all measured properties of these walls are quite consistent with a CDM–like initial power spectrum and Gaussian distribution of perturbations.

6. Possible rich clusters of galaxies

The SDSS DR1 also contains a number of galaxy complexes of various richnesses which can be extracted by means of the MST technique. Due to the large velocity dispersion of galaxies within clusters and the strong 'Finger of God' effect, this extraction must be performed using different threshold linking lengths in the radial (l_r) and in the transverse (l_t) directions. This is not unlike how group catalogs are extracted from redshift surveys using conventional 'friends-of-friends' algorithms (Huchra & Geller 1982; Tucker et al. 2000).

We performed this cluster-finding in two major steps. First, we projected the observed samples onto a sphere of radius $R = 100h^{-1}$Mpc with a random scatter $\pm 0.5h^{-1}$Mpc and extracted a set of candidate clusters from this catalog using a linking length of $r_t = 0.3h^{-1}$Mpc. Second, we applied a radial linking length of $r_r = 3h^{-1}$Mpc to these candidate clusters using their real 3D coordinates. In this second step, we also employed the threshold richness, $N_{mem} = 10$, for our final samples of possible rich complexes. Having extracted these probable rich "clusters", we calculated a distance-independent measure of their richnesses by correcting their observed richnesses N_{mem} for radial selection effects using equation (1); we call this corrected richness N_{sel}. Further discrimination of the "clusters" can be performed using their size in transverse and radial directions as well as other characteristics of selected galaxies.

For the threshold parameters used 20, 12, 43 and 10 possible rich clusters were selected from the S_1, S_2, N_1 & N_2 samples, respectively. The majority of these "clusters" are embedded within richer walls. Let us remember that these are *possible* rich clusters of galaxies and to confirm that they are physical potential wells, it is necessary to check for diffuse x-ray emission. However, comparison with the list of NORAS survey (Böhringer et al. 2000) shows that only ~ 32 of them can be roughly related to the x-ray sources. This means that the method of cluster identification must be essentially improved.

7. Mass function of the structure elements

The richness of the SDSS DR1 allows one to extract several different sets of high density clouds and structure elements with various overdensities within the HDRs and LDRs and to find their mass function. These results can be directly compared with the theoretical expectations of DD02. However, the richness of the SDSS DR1 does not yet allow one to estimate quantitatively the divergence between the expected and observed mass functions plotted in Fig. 6.

Two samples of high density galaxy groups and two samples of unrelaxed structure elements – walls and filaments – were selected separately within HDRs and LDRs introduced in Sec. 3.3 for a threshold richness $N_{mem} \geq 5$. Since the velocity dispersions in groups are expected to be much smaller than those in rich clusters, we select these samples of structure elements using the simpler method described in Sec. 4 rather than the two-step approach described in Sec. 6. The richness of each cluster was corrected for radial selection effects using the selection function introduced in Sec. 2.1.

The main properties of the selected clouds are listed in Table 2, where r_{lnk} and $\langle\delta\rangle$ are, respectively, the threshold linking length and the mean overdensity of clouds, f_{gal} is the fraction of galaxies from the total (combined HDR+LDR) sample of galaxies within the selected clouds, N_{cl} is the number of clouds while $\langle M\rangle$ and $\langle M_{sel}\rangle$ are the observed and corrected for the selection effect mean richness of individual clouds.

Results listed in Table 2 illustrate the influence of environment on the properties of high density clouds. In particular, in spite of the approximately equal number of galaxies in HDRs and LDRs, $\sim$85% and $\sim$70% of the high density clouds selected with linking lengths $r_{lnk} = 0.8$ & $1.2h^{-1}$Mpc are situated within the HDRs and accumulate $\sim$90% and $\sim$80% of galaxies. At linking length $r_{lnk} = 1.8h^{-1}$Mpc the numbers of clouds selected within HDRs and LDRs are comparable but again $\sim$80% of galaxies related to these clouds are concentrated within HDRs. At the largest linking lengths listed in Table 2 essential differences are seen only for the mean masses and number of structure elements selected within HDRs and LDRs. These differences are enhanced by the influence of the selection effect which is stronger for the LDRs.

The mass functions for these samples are plotted in Fig. 6. As was shown in DD02, in Zel'dovich theory and for the WDM initial power spectrum the dark matter mass function of structure elements is independent of their shapes and, at small redshifts, it can be approximated by the functions

$$xN(x)dx = 12.5\kappa_{ZA}x^{2/3}\exp(-3.7x^{1/3})\ \mathrm{erf}(x^{2/3})dx\,, \quad (26)$$

$$xN(x)dx = 8.\kappa_{ZA}x^{1/2}\exp(-3.1x^{1/3})\ \mathrm{erf}(x^{3/4})dx\,. \quad (27)$$

$$x = \mu_{ZA}\frac{M}{\langle M\rangle}\,,$$

The expression (26) relates to clouds which have become essentially relaxed and static by $z = 0$, and the expression (27) relates to richer, unrelaxed filaments and walls which are still in the process of collapse. Here, $\kappa_{ZA} \sim 1.5 - 4$ and $\mu_{ZA} \sim 0.8 - 1.3$ are fit parameters which take into account the incompleteness of selected samples of clouds for small and large richnesses; this incompleteness changes both the amplitude and mean mass of the measured clouds. Comparison with simulations (DD02) has shown that these relations fit reasonably well to the mass distribution of DM structure elements.

These relations are similar to the mass function from the Press– Schechter formalism,

$$xN_{PS}(x)dx = \frac{8\kappa_{PS}}{45\sqrt{\pi}}\ \xi^{1/6}\exp(-\xi^{1/3})dx\,, \quad (28)$$

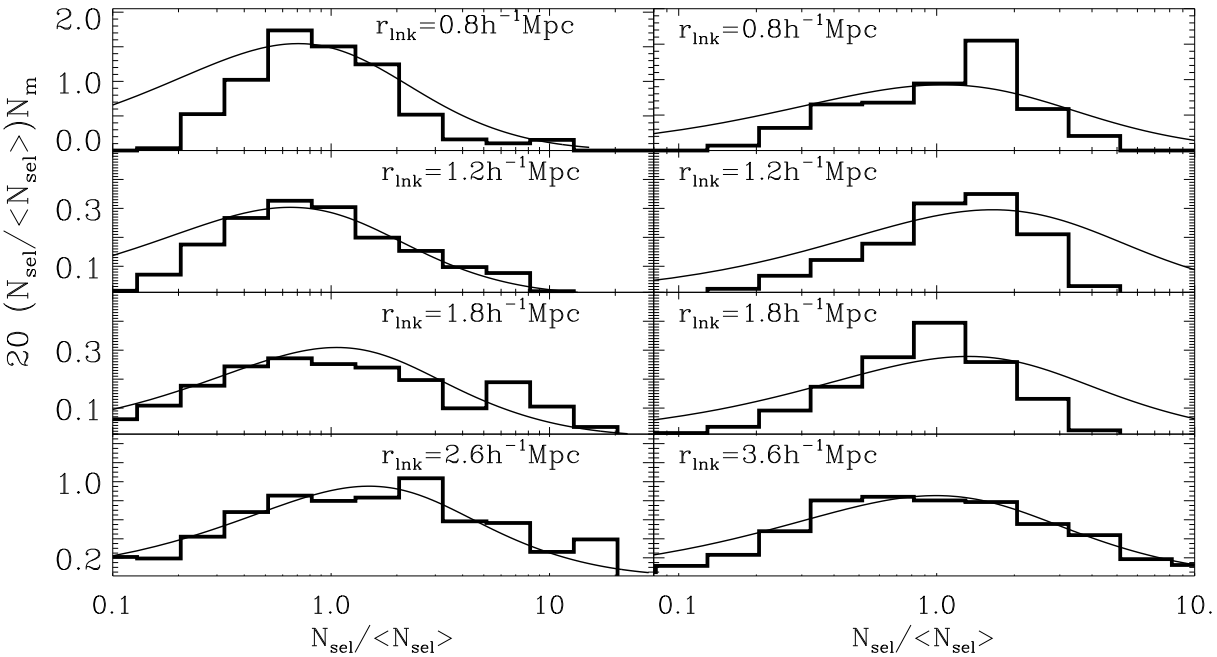

Fig. 14. Mass functions of galaxy clouds, $N_m \cdot N_{mem}/\langle N_{mem}\rangle)$, selected in HDRs (left panels) and LDRs (right panels) for four threshold linking lengths. Theoretical fit (26) for relaxed clouds ($r_{lnk} = 0.8\&1.2h^{-1}$ Mpc) and fit (27) for unrelaxed clouds ($r_{lnk} \geq 1.8h^{-1}$ Mpc) are plotted by solid lines.

Table 2. Parameters of groups of galaxies selected in HDRs and LDRs after correction for the selection effect.

$r_{lnk}h^{-1}$Mpc	$\langle\delta\rangle$	f_{gal}	N_{cl}	$\langle M\rangle$	$\langle M_{sel}\rangle$
		HDR			
0.8	140	0.1	1 193	6.8	12
1.2	40	0.24	1 961	9.5	25
1.8	10	0.39	1 731	17.7	61
2.6	3	0.47	614	61.5	228
		LDR			
0.8	220	0.014	220	4.8	14
1.2	61	0.05	817	5.3	18
1.8	16	0.15	1 805	6.4	36
3.6	3	0.36	2 295	12.5	106

$$\xi = 1.785\mu_{ps}x = 1.785\mu_{ps}M/\langle M\rangle\,,$$

despite the fact that they use different assumptions about the process of cloud formation and the shape of the formed clouds. Here again the fitting parameters κ_{PS} and μ_{PS} take into account the incompleteness of measured sample. However, this expression relates to the CDM-like power spectrum without small scale cutoff which is linked, for example, with the finite mass of DM particles, and without correction for the survival probability. So, it describes only the massive part of the mass function.

Relations (26), & (27) characterize the mass distribution of dark matter clouds associated with the observed galaxy groups and massive structure elements. They are closely linked with the initial power spectrum and fit reasonably well the observed mass distribution. For $N_{sel} \leq \langle N_{sel}\rangle$ the incompleteness of the sample of selected clouds leads to rapid drops in the observed mass functions as compared with theoretical expectations. For filaments selected within LDRs at $r_{lnk} \leq 2$ the deficit of richer clouds is enhansed by the method of filament separation. However, for the largest linking lengths, $r_{lnk} = 2.6$ & $3.6h^{-1}$Mpc, where the incompleteness and other distortions are minimal, the observed mass distribution is quite consistent with theoretical expectations.

8. Summary and discussion

Statistical analysis of large galaxy redshift surveys allows us to obtain the quantitative characteristics of the large scale galaxy distribution, which in turn can be related to the fundamental characteristics of the Universe and the processes of structure formation. The large homogeneous data set compiled in the SDSS DR1 also permits us to checking the results from analysis of the LCRS and the DURS and to obtain more accurate and more representative estimates of the main basic characteristics of the Universe.

The spatial galaxy distribution for the S_1 samples is plotted in Fig. 15; galaxies in HDRs are highlighted.

8.1. Main results

The main results of our investigation can be summarized as follows:

1. The analysis performed in Sec. 3 with the MST technique confirms that about half of galaxies are situated within rich wall–like structures and the majority of the

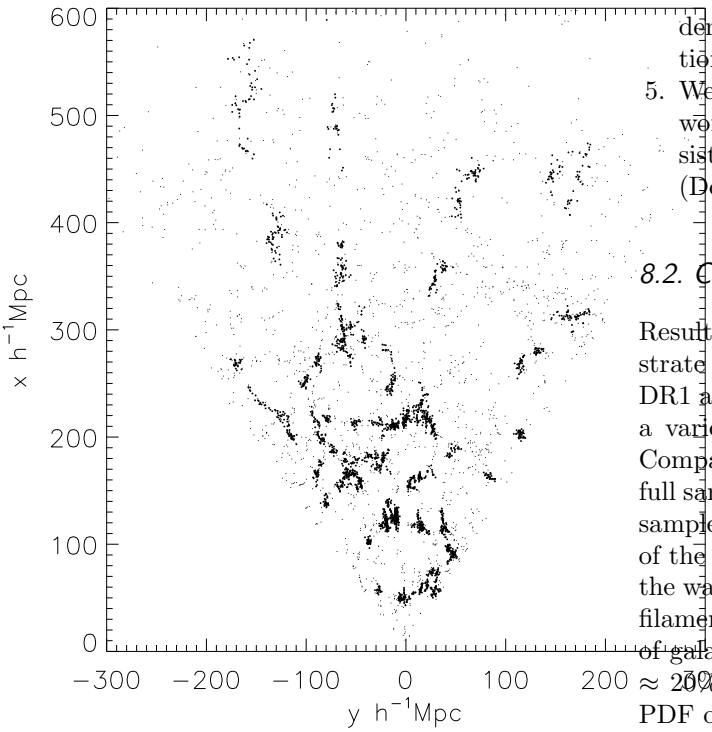

Fig. 15. Spatial distribution of all galaxies in the S_1 sample (points) and within the HDRs (thick points).

remaining galaxies are concentrated within filaments. This result confirms that the filaments and walls are the main structure elements in the observed galaxy distribution. Quantitative characteristics of walls and filaments presented in Sections 3, 4 & 5 validate this division of the LSS into these two subpopulations.

2. The main characteristics of wall–like structure elements, such as the overdensity, separation distance between walls, wall thickness, and the velocity dispersion within walls, were measured separately for radial and, for the SDSS DR1 equatorial stripes, in transverse directions. Comparison of these characteristics demonstrates that the walls are approximately in static equilibrium, that they are relaxed along their shorter axis, and that their observed thickness in the radial direction is defined by the velocity dispersion of galaxies.
3. The PDF of the wall surface density is consistent with the simulated one and with that predicted by Zel'dovich theory for Gaussian initial perturbations and CDM–like initial power spectrum. The measured amplitude of perturbations coincides with that expected for the spatially flat ΛCDM cosmological model with $\Omega_\Lambda \approx 0.7$ and $\Omega_m \approx 0.3$. These results demonstrate that the spatial galaxy distribution traces the dark matter distribution nicely.
4. The mass distributions of groups of galaxies, filaments and walls selected with various threshold overdensities nicely fit the joint mass function consistent with the expectations of Zel'dovich theory. Characteristics of these groups of galaxies listed in Table 2 clearly demonstrate the impact of environment and interaction of small and large scale perturbations.
5. We found the typical cell size of the filamentary network to be $\sim 10h^{-1}$Mpc (Sec. 4). This estimate is consistent with the one obtained previously for the LCRS (Doroshkevich et al. 1996, 2001).

8.2. Characteristics of the LSS

Results obtained in Sec. 3 with the MST technique demonstrate that at least 80 – 90% of galaxies in the SDSS DR1 are concentrated within the filaments and walls with a variety of richness and overdensity forming the LSS. Comparison of the mean edge lengths (6, 8 and 9) for the full sample, HDRs and LDRs with the mean density of the sample (3) shows that the LSS occupies only roughly half of the volume. It also shows that the mean overdensity of the walls is larger than 10. The same results show that the filaments are formed by a system of high density groups of galaxies which contain ≈ 30% of all galaxies. For only ≈ 20% of galaxies do we see the actual one dimensional PDF of the MST edge lengths (Fig. 5).

There is continuous distribution in morphology and richness of the LSS elements. It can be roughly described as a system of walls randomly distributed in space with mean separations of $\approx (50 \pm 10)h^{-1}$Mpc and a filamentary network connected to the walls. The typical size of lower density regions, or voids, situated between filaments and walls is estimated in Sec. 4 as approximately 10–12 h^{-1}Mpc.

These results agree with those obtained for the mock catalogues simulating the galaxy distribution and indicate that galaxies nicely trace the spatial distribution of dominated dark matter.

8.3. Properties of walls and parameters of the initial power spectrum

Walls and filaments are the largest structure elements observed in the Universe. In contrast to galaxies, their formation occurs at relatively small redshifts in course of the last stage of nonlinear matter clustering and is driven by the initial power spectrum of perturbations. Therefore, their properties can be successfully described by the nonlinear theory of gravitational instability (Zel'Dovich 1970) that allows us to link them with the characteristics of the initial power spectrum.

The interpretation of the walls as Zel'dovich pancakes has been discussed already in Thompson & Gregory (1978) and in Oort (1983). The comparison of the statistical characteristics of the Zel'dovich pancakes for a CDM–like initial power spectrum (DD99, DD02) with those for observed walls demonstrates that, indeed, this interpretation is correct and, for a given cosmological model, it allows us to obtain independent estimates of the fundamental characteristics of the initial power spectrum.

The estimates of the mean wall surface density, $\langle q_w \rangle$, and the amplitude of initial perturbations, $\langle \tau_m \rangle$, listed in Table 1 are consistent with each other and with those found for the LCRS and DURS. They are also close to those found for the simulated DM distribution and for the mock galaxy catalogs (Cole et al. 1998) prepared for a spatially flat ΛCDM cosmological model with $\Omega_\Lambda = 0.7$, $\Omega_m = 0.3$ and $\sigma_8 = 1.05$. As was shown in Sec. 5.3 (20), (21) and (22), the PDFs of both observed and simulated wall surface density plotted in Figs. 10 and 11 coincide with those theoretically expected (15) for Gaussian initial perturbations with a CDM–like power spectrum (DD99; DD02).

Averaging of both $\langle q_w \rangle$ and $\langle \tau_m \rangle$ listed in Table 1 allows us to estimate the mean values as follows:

$$\langle q_w \rangle = (0.38 \pm 0.06)(\Gamma/0.2)\,, \tag{29}$$

$$\tau_m = (0.24 \pm 0.02)\sqrt{\Gamma/0.2}\,. \tag{30}$$

These values are consistent with the best estimates of the same amplitude (Spergel et al. 2003) for the ΛCDM cosmological model with $\Gamma = 0.2$

$$\sigma_8 \approx 0.9 \pm 0.1, \quad \tau \approx 0.22 \pm 0.02\,, \tag{31}$$

These results verify that galaxies nicely trace the LSS formed mainly by the dark matter distribution and the observed walls are recently formed Zel'dovich pancakes. They also verify the Gaussian distribution of initial perturbations and coincide with the Harrison – Zel'dovich primordial power spectrum.

Comparison of other wall characteristics measured in radial and transverse directions indicate that the walls are gravitationally confined and relaxed along the shorter axis. The same comparison allows us to find the true wall overdensity, wall thickness, and the radial velocity dispersion of galaxies within walls. As is seen from relation (18), these values are quite self–consistent.

8.4. Mass function of structure elements

The samples of walls, filaments, and groups of galaxies in the SDSS DR1 selected using different threshold overdensities allow us to measure their mass functions, to trace their dependence on the threshold overdensity and environment, and to compare them with the expectations of Zel'dovich theory.

This comparison verifies that for lower threshold overdensities for both filaments and wall–like structure elements, the shape of the observed mass functions is consistent with the expectations of Zel'dovich theory. However, for high density groups of galaxies some deficit of low mass groups caused, in particular, by selection effects and enhanced by the restrictions inherent in our procedure for group-finding leads to a stronger difference between the observed and expected mass functions for $M_{sel} \le \langle M_{sel} \rangle$. The same factors distort the observed mass functions for groups selected within LDRs.

Let us note that mass functions (26, 27, & 28) are closely linked with the initial power spectrum. This is manifested as a suppression of the PDFs at $M_{sel} \le \langle M_{sel} \rangle$ and is proportional to $\exp[-(M/\langle M_{sel} \rangle)^{1/3}]$ at $M_{sel} \ge \langle M_{sel} \rangle$. They differ from the mass function of galaxy clusters and the probable mass function of observed galaxies which are formed on account of multi–step merging of less massive clouds and are described by a power law with a negative power index at $M_{sel} \le \langle M_{sel} \rangle$ and an exponential cutoff $\propto \exp[-(M/\langle M_{sel} \rangle)$ at $M_{sel} \ge \langle M_{sel} \rangle$ (see e.g. Silk & White 1978).

8.5. Interaction of large and small scale perturbations

The data listed in Table 2 shows that the majority of high density groups of galaxies and the main fraction of galaxies related to these groups (up to 80 – 90%) are situated within HDRs. These results illustrate the influence of environment on galaxy formation and the clustering of luminous matter. It also indicates the importance of interactions of small and large scale perturbations for the formation of the observed LSS. This problem was also discussed in Einasto et al. (2003a,b).

These differences are partly enhanced by the influence of selection effects. Indeed, the majority of HDRs are situated at moderate distances $D \sim 150 - 300h^{-1}$Mpc where this influence is not so strong. On the other hand the LDRs also include all galaxies situated in the farthest low density regions. However, as was shown in DD02 significant differences between the characteristics of clouds separated within HDRs and LDRs is seen even for simulated clustering of dark matter.

These results are consistent with the high concentration of observed galaxies within the filaments and walls forming the LSS noted in Sec. 8.2. Bearing in mind that the mean density of luminous matter does not exceed 10% of the full matter density of the Universe we can conclude that galaxies are formed at high redshifts presumably within compressed regions which are now seen as elements of LSS.

A natural explanation for both of these differences and the high concentration of galaxies within the LSS elements is the interaction of small and large scale perturbations when large scale compression of matter accelerates the formation of small scale high density clouds. Such interactions may also explain the existence of large voids similar to the Böotes void where formation of galaxies has been strongly suppressed.

8.6. Possible rich clusters of galaxies

The MST technique generalizes the standard 'friends–of–friends' method of the selection of denser clouds and of probable clusters of galaxies. However, first attempts of such selection presented in Sec. 6 show that there is an essential difference between the selected high density clouds and x-ray sources. The nature of this difference is not yet

clear and perhaps it will be eliminated after the introduction of stronger criteria for the selection of probable clusters of galaxies from the survey.

8.7. Final comments

The SDSS (York et al. 2000; Stoughton et al. 2002; Abazajian et al. 2003) and 2dF (Colless et al. 2001) galaxy redshift surveys provide deep and broad vistas with which cosmologists may study the galaxy distribution on extremely large scales –scales on which the imprint from the primordial fluctuation spectrum has not been erased.

In this paper, we have used the SDSS DR1 to investigate the galaxy distribution at such large scales. We have confirmed our earlier results, based on the LCRS and DURS samples, that galaxies are distributed in roughly equal numbers between two different environments: filaments, which dominate low density regions, and walls, which dominate high density regions. Although different in character, these two environments together form a fragmented joint random network of galaxies – the cosmic web.

Comparison with theory strongly supports the idea that the properties of the observed walls are consistent with those for Zel'dovich pancakes formed from a Gaussian spectrum of initial perturbations for a flat ΛCDM Universe ($\Omega_\Lambda \approx 0.7$, $\Omega_m \approx 0.3$). These results are consistent with the estimate of $\Gamma = 0.20 \pm 0.03$ obtained in Percival et al. (2001) for the 2dF Galaxy Redshift Survey (see also Spergel et al. 2003).

Such analysis one allows to obtain some important basic conclusions regarding the properties and the process of formation and evolution of the large scale structure of the Universe. With future public releases of the SDSS data set, we hope to refine these conclusions.

Acknowledgments

We thank Shiyin Shen of the Max-Planck-Institut für Astrophysik and Jörg Retzlaff of the Max-Planck-Institut für Extraterrestrial Physics for useful discussions regarding this work.

Funding for the creation and distribution of the SDSS Archive has been provided by the Alfred P. Sloan Foundation, the Participating Institutions, the National Aeronautics and Space Administration, the National Science Foundation, the US Department of Energy, the Japanese Monbukagakusho, and the Max Planck Society. The SDSS Web site is http://www.sdss.org/.
The Participating Institutions are the University of Chicago, Fermilab, the Institute for Advanced Study, the Japan Participation Group, the Johns Hopkins University, the Max Planck Institute for Astronomy (MPIA), the Max Planck Institute for Astrophysics (MPA), New Mexico State University, Princeton University, the United States Naval Observatory, and the University of Washington.
This paper was supported in part by Denmark's Grundforskningsfond through its support for an establishment of the Theoretical Astrophysics Center.

References

Abazajian, K., Adelman–McCarthy, J. K., Agüeros, M. A., Allam, S. S., & the SDSS Collaboration. 2003, ArXiv Astrophysics e-prints, 5492
Böhringer, H., Voges, W., Huchra, J. P., McLean, B., Giacconi, R., Rosati, P., Burg, R., Mader, J., Schuecker, P., Simiç, D., Komossa, S., Reiprich, T. H., Retzlaff, J., & Trümper, J. 2000, ApJS, 129, 435
Barrow, J. D., Bhavsar, S. P., & Sonoda, D. H. 1985, MNRAS, 216, 17
Baugh, C. M. & Efstathiou, G. 1993, MNRAS, 265, 145
Bhavsar, S. P. & Ling, E. N. 1988, ApJ, 331, L63
Buryak, O. & Doroshkevich, A. 1996, A&A, 306, 1
Cole, S., Hatton, S., Weinberg, D. H., & Frenk, C. S. 1998, MNRAS, 300, 945
Colless, M., Dalton, G., Maddox, S., Sutherland, W., Norberg, P., Cole, S., Bland-Hawthorn, J., Bridges, T., Cannon, R., Collins, C., Couch, W., Cross, N., Deeley, K., De Propris, R., Driver, S. P., Efstathiou, G., Ellis, R. S., Frenk, C. S., Glazebrook, K., Jackson, C., Lahav, O., Lewis, I., Lumsden, S., Madgwick, D., Peacock, J. A., Peterson, B. A., Price, I., Seaborne, M., & Taylor, K. 2001, MNRAS, 328, 1039
Demiański, M. & Doroshkevich, A. G. 1999, MNRAS, 306, 779
—. 2002, ArXiv Astrophysics e-prints, 6282
Demiański, M., Doroshkevich, A. G., & Turchaninov, V. 2000, MNRAS, 318, 1189
—. 2003, MNRAS, 340, 525
Doroshkevich, A. G., Fong, R., McCracken, H. J., Ratcliffe, A., Shanks, T., & Turchaninov, V. I. 2000, MNRAS, 315, 767
Doroshkevich, A. G., Tucker, D. L., Fong, R., Turchaninov, V., & Lin, H. 2001, MNRAS, 322, 369
Doroshkevich, A. G., Tucker, D. L., Oemler, A. J., Kirshner, R. P., Lin, H., Shectman, S. A., Landy, S. D., & Fong, R. 1996, MNRAS, 283, 1281
Einasto, M., Einasto, J., Müller, V., Heinämäki, P., & Tucker, D. L., 2003, A&A, 401, 851
Einasto, J., Hútsi, G., Einasto, M., Saar, E., Tucker, D. L., Müller, V., Heinämäki, P., & Allam, S. S. 2003, A&A, 405, 425
Fukugita, M., Ichikawa, T., Gunn, J. E., Doi, M., Shimasaku, K., & Schneider, D. P. 1996, AJ, 111, 1748
Gunn, J. E., Carr, M., Rockosi, C., Sekiguchi, M., & the SDSS Collaboration. 1998, AJ, 116, 3040
Huchra, J. P. & Geller, M. J. 1982, ApJ, 257, 423
Jenkins, A., Frenk, C. S., Pearce, F. R., Thomas, P. A., Colberg, J. M., White, S. D. M., Couchman, H. M. P., Peacock, J. A., Efstathiou, G., & Nelson, A. H. 1998, ApJ, 499, 20
Kruskal, J. B. 1956, Proc. Amer. Math. Soc., 7, 48
Oort, J. H. 1983, ARA&A, 21, 373
Percival, W. J., Baugh, C. M., Bland-Hawthorn, J., Bridges, T., Cannon, R., Cole, S., Colless, M., Collins, C., Couch, W., Dalton, G., De Propris, R., Driver, S. P.,

Efstathiou, G., Ellis, R. S., Frenk, C. S., Glazebrook, K., Jackson, C., Lahav, O., Lewis, I., Lumsden, S., Maddox, S., Moody, S., Norberg, P., Peacock, J. A., Peterson, B. A., Sutherland, W., & Taylor, K. 2001, MNRAS, 327, 1297

Prim. 1957, Bell System Tech. J., 36, 1389

Ratcliffe, A., Shanks, T., Broadbent, A., Parker, Q. A., Watson, F. G., Oates, A. P., Fong, R., & Collins, C. A. 1996, MNRAS, 281, L47+

Schmalzing, J., Gottlöber, S., Klypin, A. A., & Kravtsov, A. V. 1999, MNRAS, 309, 1007

Shandarin, S. F. & Zeldovich, Y. B. 1989, Reviews of Modern Physics, 61, 185

Shectman, S. A., Landy, S. D., Oemler, A., Tucker, D. L., Lin, H., Kirshner, R. P., & Schechter, P. L. 1996, ApJ, 470, 172

Sheth, J. V., Sahni, V., Shandarin, S. F., & Sathyaprakash, B. S. 2002, ArXiv Astrophysics e-prints, 10136

Silk, J. & White, S. D. 1978, ApJl, 223, L59

Spergel, D. N., Verde, L., Peiris, H. V., Komatsu, E., Nolta, M. R., Bennett, C. L., Halpern, M., Hinshaw, G., Jarosik, N., Kogut, A., Limon, M., Meyer, S. S., Page, L., Tucker, G. S., Weiland, J. L., Wollack, E., & Wright, E. L. 2003, ArXiv Astrophysics e-prints, 2209

Stoughton, C., Lupton, R. H., Bernardi, M., Blanton, M. R., & the SDSS Collaboration. 2002, AJ, 123, 485

Thompson, L. A. & Gregory, S. A. 1978, ApJ, 220, 809

Tucker, D. L., Oemler, A. J., Hashimoto, Y., Shectman, S. A., Kirshner, R. P., Lin, H., Landy, S. D., Schechter, P. L., & Allam, S. S. 2000, ApJS, 130, 237

van de Weygaert, M. A. M. 1991, Ph.D Thesis (Leiden: Rijksuniversiteit, —c1991)

York, D. G., Adelman, J., Anderson, J. E., Anderson, S. F., & the SDSS Collaboration. 2000, AJ, 120, 1579

Zel'Dovich, Y. B. 1970, A&A, 5, 84